JACS
JOURNAL OF THE AMERICAN CHEMICAL SOCIETY
pubs.acs.org/JACS
Article

An $[Fe_4S_4]^{3+}$–Alkyl Cluster Stabilized by an Expanded Scorpionate Ligand

Alex McSkimming, Arun Sridharan, Niklas B. Thompson, Peter Müller, and Daniel L. M. Suess*

Cite This: J. Am. Chem. Soc. 2020, 142, 14314–14323
Read Online

ABSTRACT: Alkyl-ligated iron–sulfur clusters in the $[Fe_4S_4]^{3+}$ charge state have been proposed as short-lived intermediates in a number of enzymatic reactions. To better understand the properties of these intermediates, we have prepared and characterized the first synthetic $[Fe_4S_4]^{3+}$–alkyl cluster. Isolation of this highly reactive species was made possible by the development of an expanded scorpionate ligand suited to the encapsulation of cuboidal clusters. Like the proposed enzymatic intermediates, this synthetic $[Fe_4S_4]^{3+}$–alkyl cluster adopts an $S = {}^1/_2$ ground state with $g_{iso} > 2$. Mössbauer spectroscopic studies reveal that the alkylated Fe has an unusually low isomer shift, which reflects the highly covalent Fe–C bond and the localization of Fe^{3+} at the alkylated site in the solid state. Paramagnetic ^1H NMR studies establish that this valence localization persists in solution at physiologically relevant temperatures, an effect that has not been observed for $[Fe_4S_4]^{3+}$ clusters outside of a protein. These findings establish the unusual electronic-structure effects imparted by the strong-field alkyl ligand and lay the foundation for understanding the electronic structures of $[Fe_4S_4]^{3+}$–alkyl intermediates in biology.

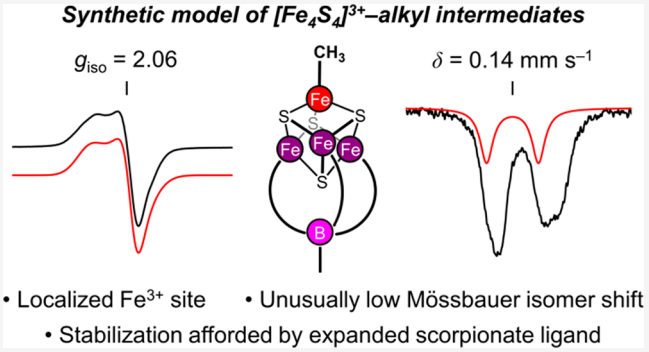

INTRODUCTION

Iron–sulfur (Fe–S) enzymes perform diverse cellular functions including kinetically challenging reactions that proceed via transient intermediates.[1−4] Characterization of such intermediates often requires low-temperature trapping and manipulation, which can preclude analysis of their properties at physiologically relevant temperatures and crystallographic experiments.[5−8] For this reason, it is crucial to be able to compare their spectroscopic features with those of well-defined model complexes. Indeed, insights into the mechanisms and properties of Fe–S enzymes have been fueled by a decades-long synergy between synthetic chemistry, biochemistry, and spectroscopy.[2,9−15] Despite these advances, synthetic Fe–S cluster chemistry has mostly yielded information about the geometric and electronic properties of resting-state species,[2,12−15] and preparing well-defined models of reactive intermediates remains an ongoing challenge.

In particular, alkylated $[Fe_4S_4]^{3+}$ species are now thought to be intermediates in a variety of reactions performed by Fe–S enzymes, including steps in terpene biosynthesis,[7,16−19] radical initiation in the >100 000 members of the radical SAM enzyme superfamily,[8,20−24] and a critical C–C bond-forming step in diphthamide biosynthesis[25] (Scheme 1). In all cases, they are transient species trapped in rapid freeze-quench experiments. They are also thought to have diverse structures and reactivity patterns. For example, it has been proposed that the Fe–C bond in a ferraoxetane intermediate in terpene biosynthesis breaks heterolytically upon reduction of the $[Fe_4S_4]^{3+}$ state (Scheme 1A),[7] whereas the Fe–C bonds in intermediates in canonical and noncanonical radical SAM enzymes have been proposed to undergo homolysis (Scheme 1B and C).[8,23,24] Moreover, the structures and spectroscopic properties of $[Fe_4S_4]^{3+}$–alkyl species in radical SAM enzymes can depend on the method of their generation (i.e., by thermal or photochemical methods).[24,26] Understanding the basis for their diverse properties will require knowledge of their underlying electronic structures, particularly how (if at all) the valence-electron distribution is perturbed by the alkyl ligand, and this will rely on synthetic access to well-defined $[Fe_4S_4]^{3+}$–alkyl clusters whose structures, properties, and reactivity can be thoroughly and systematically studied.

As a first step toward understanding the electronic structure and reaction chemistry of alkylated Fe_4S_4 clusters, we recently reported the synthesis and characterization of an $[Fe_4S_4]^{2+}$–alkyl cluster (**1**) supported by the tridentate ligand $L(NP)_3$

Received: June 11, 2020
Published: July 21, 2020

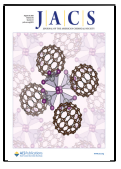

Scheme 1. Proposed $[Fe_4S_4]^{3+}$–Alkyl Intermediates Characterized by EPR Spectroscopy during Turnover of (A) IspG and (B,C) Radical SAM Enzymes[a]

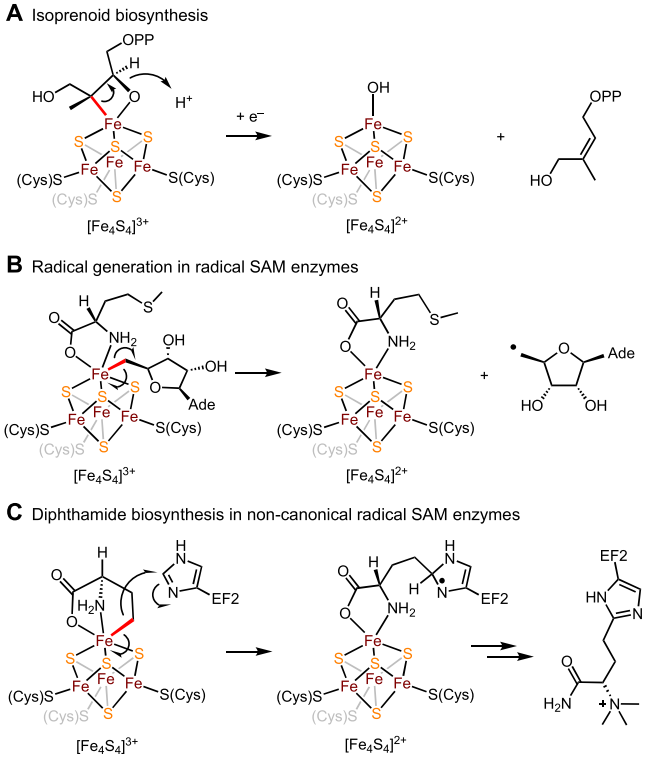

[a]Ade = adeninyl, EF2 = Elongation Factor 2, $[Fe_4S_4]^{n+}$ refers to an Fe_4S_4 cluster with a core charge of n^+.

(Scheme 2A).[27] Spectroscopic and crystallographic analyses of this compound provided insights into how the alkyl group at the unique Fe site perturbs the double-exchange interactions in the cubane, but it was not clear if and how these properties would extend to the one-electron-oxidized $[Fe_4S_4]^{3+}$ redox state, the only redox state in which Fe_4S_4–alkyl clusters have been observed in biology.[7,8,18,19,23−26] Attempts to generate an $[Fe_4S_4]^{3+}$–alkyl cluster by oxidation of **1** have been unsuccessful; only decomposition and intractable mixtures of products have been obtained. Oxidation of the analogous alkylated cluster **2** bound by the imidazolinimine ligand $L(NIm)_3$ (Scheme 2A) gave cleaner reaction mixtures (see the Supporting Information); however, the products proved resistant to isolation and decomposed upon manipulation. These preliminary results and the aforementioned enzymatic studies suggested that $[Fe_4S_4]^{3+}$–alkyl clusters may be exceptionally reactive. Indeed, synthetic $[Fe_4S_4]^{3+}$ clusters are generally more difficult to isolate than $[Fe_4S_4]^{2+}$ clusters, and, to date, only a handful have been reported.[28−32] Consequently, we sought a new strategy for isolating an $[Fe_4S_4]^{3+}$–alkyl cluster. We reasoned that incorporation of a noncoordinating anion into a tridentate ligand framework would allow for the generation of an $[Fe_4S_4]^{3+}$–alkyl cluster as a monocation instead of a dication, with the decreased molecular charge rendering the cluster less electrophilic. This strategy takes inspiration from the development of borate-derived scorpionate ligands (Scheme 2B), which have been prepared with a large variety of donors and have become staples of synthetic inorganic chemistry.[33−37]

Scheme 2. (A) Attempted Oxidation of $[Fe_4S_4]^{2+}$–Alkyl Clusters Ligated by Neutral, Tridentate Iminophosphorane/Imidazolinimine Ligands; and (B) This Work: Anionic Scorpionate Ligands for Stabilizing Reactive Metalloclusters[a]

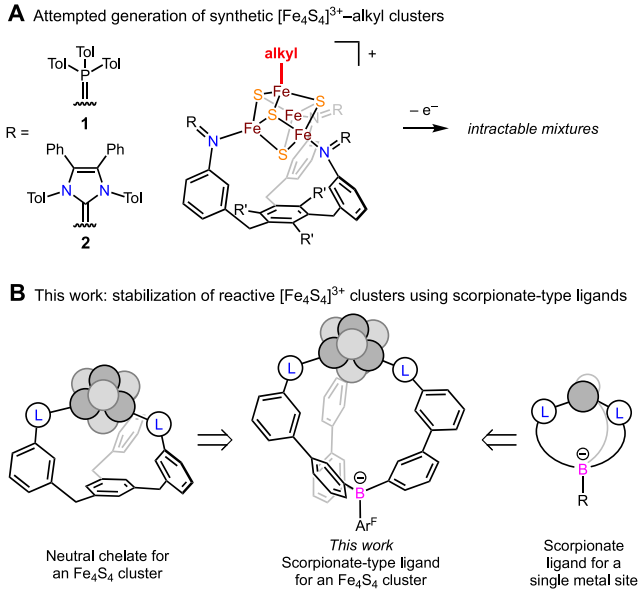

[a]R′ = Et (**1**) or H (**2**); Ar^F = 3,5-bis(trifluoromethyl)phenyl.

We herein report the design and synthesis of a tris(imidazolinimine)borate ligand that binds an Fe_4S_4 cluster in a manner nearly identical to that of $L(NIm)_3$ and thereby extends the design principles of scorpionate ligands to metalloclusters. This has enabled the preparation and characterization of the first isolable $[Fe_4S_4]^{3+}$–alkyl cluster, which, analogous to proposed enzymatic intermediates, adopts an $S = {}^1/_2$ ground state with $g_{iso} > 2$. Through crystallographic and Mössbauer spectroscopic analyses, we show that this cluster adopts a local Fe^{3+} valence at the alkylated site in the solid state with an unusually low Mössbauer isomer shift. Unlike other synthetic Fe_4S_4 clusters, this valence localization is also observed in the solution state at room temperature as indicated by paramagnetic-NMR spectroscopic analysis. These results are discussed in the context of enzymatic $[Fe_4S_4]^{3+}$–alkyl intermediates and demonstrate the utility of expanded scorpionate ligands for stabilizing reactive metalloclusters.

RESULTS AND DISCUSSION

The binding pockets created by scorpionate ligands typically feature interdonor distances of ∼3 Å for first-row, p-block elements, and are therefore too small to encapsulate a cuboidal Fe_4S_4 cluster. Holm's original work describing the structures of 3:1 site-differentiated Fe_4S_4 clusters ligated by a trithiolate ligand[38,39] and subsequent work by us[27,40] and others[41,42] establish that a tridentate ligand for an Fe_4S_4 cluster should feature interdonor distances of ∼6 Å (cf., the N−N interdonor distances of $L(NIm)_3$ and $L(NP)_3$; both average 5.9 Å).[27,40] We determined that for an expanded scorpionate ligand, linking the donor atoms to a central borate by 3,3′-biphenyl groups would allow for an appropriate interdonor distance and orientation for binding Fe_4S_4 clusters (Scheme 2B). We therefore designed and developed a synthesis of $[L^B(NIm)_3]^-$, an anionic analogue of $L(NIm)_3$ (Scheme 3). The linkers

https://dx.doi.org/10.1021/jacs.0c06334
J. Am. Chem. Soc. 2020, 142, 14314−14323

Scheme 3. Synthesis of $[^nBu_4N][L^B(NIm)_3]$[a]

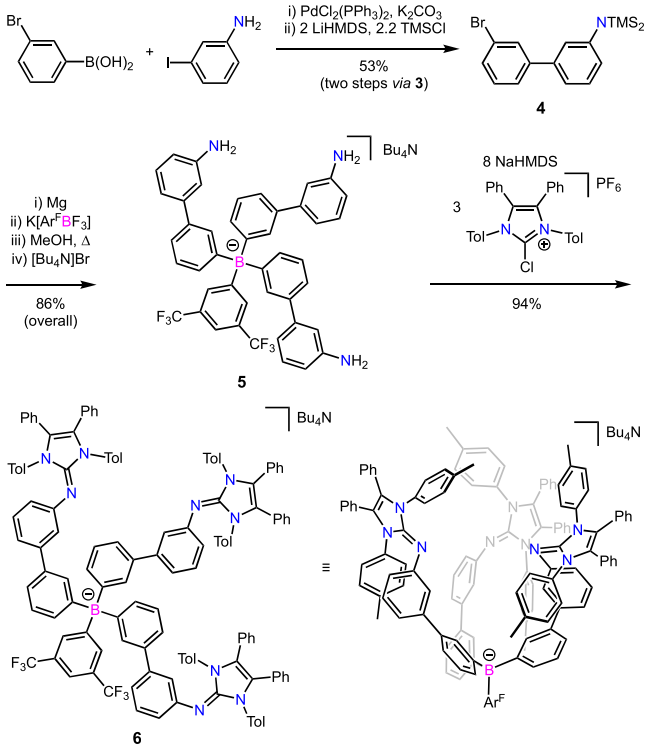

[a] Ar^F = 3,5-bis(trifluoromethyl)phenyl.

between the borate and donor atoms were constructed by Suzuki coupling of 3-iodoaniline and 3-bromoboronic acid to give 3′-bromo-3-aminobiphenyl (**3**) in 54% yield, which was protected as the bis(trimethylsilyl) derivative **4**. The corresponding Grignard reagent was prepared using Mg^0, quenched with $K[Ar^FBF_3]$ (Ar^F = 3,5-bis(trifluoromethyl)-phenyl), and deprotected in hot methanol with subsequent cation exchange to give the $[^nBu_4N]^+$ salt **5** in 86% overall yield from **4**. Finally, reaction of **5** with *N*,*N*′-di-*p*-tolyl-4,5-diphenyl-2-chloroimidazolium in the presence of NaHMDS cleanly gave $[^nBu_4N][L^B(NIm)_3]$ (**6**).

Metalation of **6** using the preassembled cluster $[Ph_4P]_2[Fe_4S_4Cl_4]$ and $Na[BAr^F_4]$ as a halide abstraction reagent gave $[L^B(NIm)_3]Fe_4S_4Cl$ (**7**) as a crystalline, red-black solid in 70% yield (Scheme 4). The use of $Na[BAr^F_4]$ enables the isolation of **7** by crystallization from a mixture of THF and Et_2O in which the byproducts, $[^nBu_4N][BAr^F_4]$ and $[Ph_4P][BAr^F_4]$, remain in solution. Treatment of **7** with MeMgCl or MeLi in coordinating solvents such as THF or Et_2O gave predominantly diamagnetic ligand degradation products and insoluble black solids. However, stirring an *o*-difluorobenzene (DFB) solution of **7** over a suspension of excess Me_2Mg cleanly generates orange-brown $[L^B(NIm)_3]Fe_4S_4CH_3$ (**8**) in 85% isolated yield. Key to the synthesis of **8** is the insolubility of Me_2Mg in DFB; reactions of **7** and Me_2Mg under homogeneous conditions invariably resulted in cluster degradation. In the absence of air and moisture, **7** and **8** are stable for prolonged periods; heating solutions in benzene at 80 °C for 24 h causes no change to their ^1H and ^{19}F NMR spectra. The room-temperature ^1H NMR spectra of **7** and **8** are similar and feature slightly broadened, paramagnetically shifted resonances (Figures S13 and S17, respectively), consistent with the expected diamagnetic ground state (formally derived from antiferromagnetic coupling of two $S = {}^9/_2$ $[2Fe^{2.5+}]$ rhombs) and some thermal population of excited states as is commonly observed for $[Fe_4S_4]^{2+}$

Scheme 4. Synthesis of $[L^B(NIm)_3]$-Ligated Fe_4S_4 Clusters Presented in This Work[a]

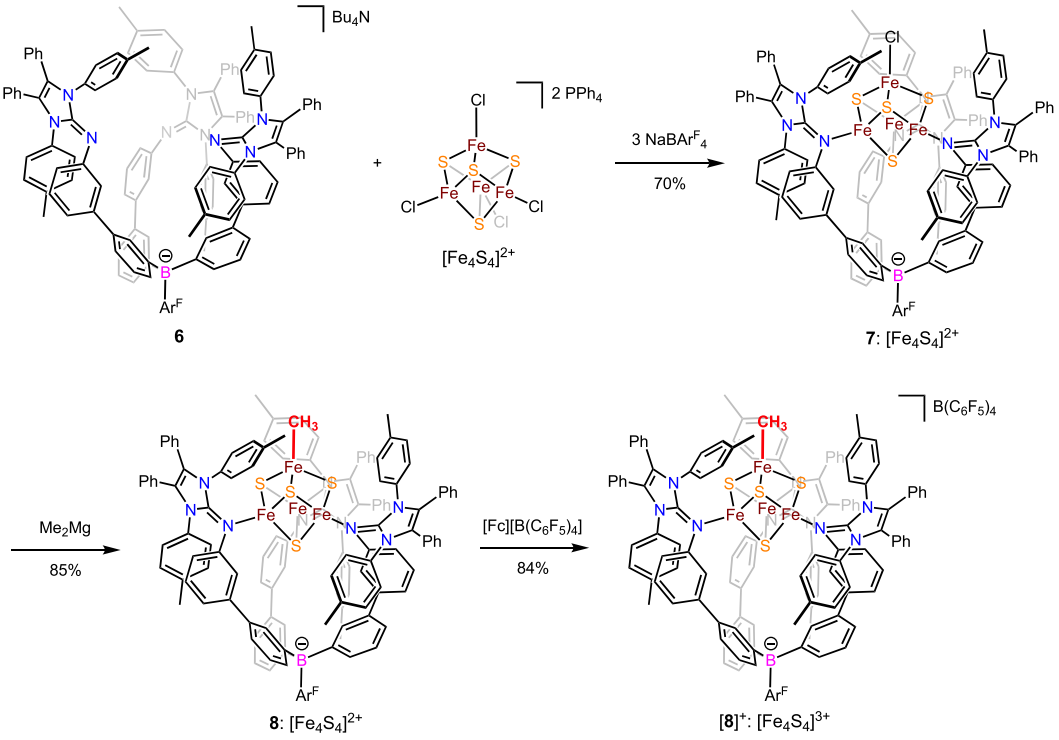

[a] Ar^F = 3,5-bis(trifluoromethyl)phenyl; Fc = ferrocene.

https://dx.doi.org/10.1021/jacs.0c06334
J. Am. Chem. Soc. 2020, 142, 14314−14323

clusters.[12,43−46] Notably, for **8**, a broad resonance is observed at 67.7 ppm that is not observed in the corresponding ^{1}H NMR spectrum of the CD_3 isotopologue (Figure S27) and was therefore assigned to the protons of the CH_3 ligand. This chemical shift is similar to that reported for the methylene protons in **1** (70.0 ppm).[27]

Single-crystal X-ray diffraction (XRD) studies of **7** and **8** establish that the $[L^B(NIm)_3]^-$ ligand binds to three Fe centers of the $[Fe_4S_4]^{2+}$ cluster core, which thereby imparts the desired 3:1 site-differentiation (Figure 1). With the exception of the

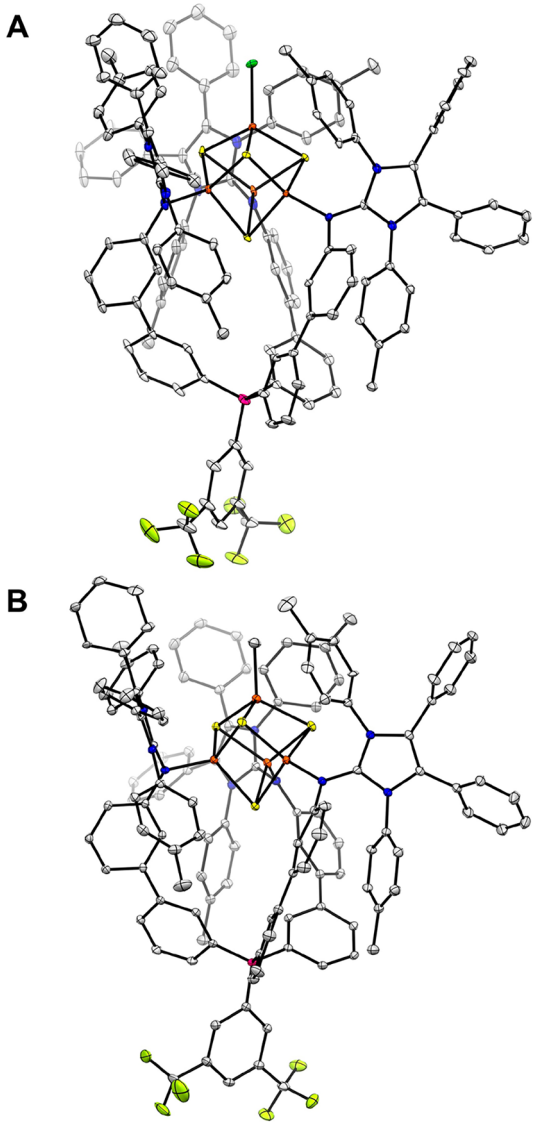

Figure 1. Thermal ellipsoid plots (30%) of $[L^B(NIm)_3]Fe_4S_4X$ with (A) X = Cl (**7**) and (B) X = CH_3 (**8**). Orange, yellow, blue, pink, green, and gray ellipsoids represent Fe, S, N, B, F, and C, respectively. Hydrogen atoms and solvent molecules are omitted for clarity.

ligand bound to the unique Fe site, the structure of cluster **8** closely resembles that of **7**. The Fe−CH_3 distance of 2.026(3) Å is similar to that observed for **1** and **2** (2.054(9) and 2.010(6) Å, respectively; see the Supporting Information for data on **2**).[27] The overall structure and metrical parameters for **8** are similar to those of the isoelectronic, cationic cluster **2** (cf., Figure 2A and B) with both featuring average interdonor N−N distances of ∼6.0 Å. In both structures, the

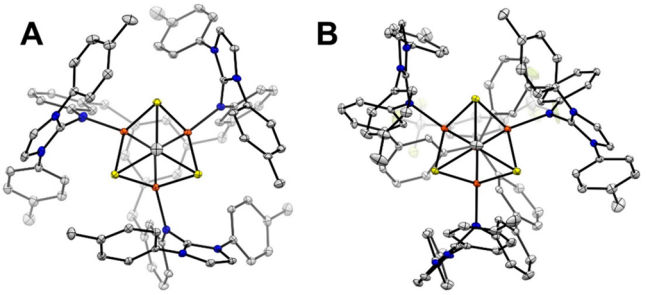

Figure 2. Top-down views from the structures of (A) $[(L(NIm)_3)Fe_4S_4CH_3]^+$ (**2**) and (B) $[L^B(NIm)_3]Fe_4S_4CH_3$ (**8**) showing the similar Fe_4S_4 coordination environments. The coloring scheme is the same as that in Figure 1. Hydrogen atoms, solvent molecules, and Ph substituents are omitted for clarity.

imidazolinimine groups are similarly tilted; in **8**, an *N*-tolyl group is accommodated within the pocket between two biphenyl linkers, and in **2**, the *N*-tolyl group fits between two phenyl linkers. These structural studies establish that the tris(biphenyl)borate framework is an anionic structural analogue of the neutral skeleton anchored by a 1,3,5-trisubstituted benzene ring that was developed by Holm and has since been adapted by us and others.[27,38−42,47]

Having developed preparations of **7** and **8**, we assessed the accessibility of the $[Fe_4S_4]^{3+}$ redox state using cyclic voltammetry. The cyclic voltammograms of **7** and **8** are similar (Figure 3) and feature two one-electron processes

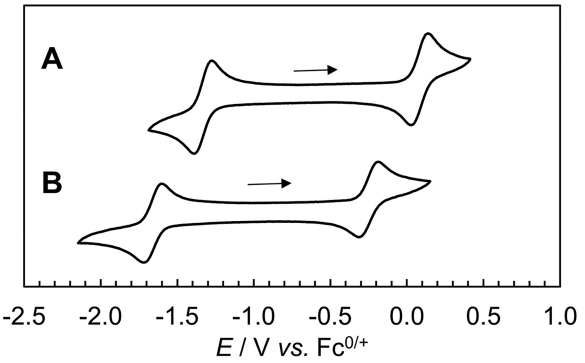

Figure 3. Cyclic voltammagrams recorded for $[L^B(NIm)_3]Fe_4S_4X$ with (A) X = Cl (**7**) and (B) X = CH_3 (**8**). Conditions: 2 mM in *o*-difluorobenzene−$[^nPr_4N][BAr^F_4]$ at 100 mV s^{-1}. Fc = ferrocene.

(Figures S45 and S46) assigned to the $[Fe_4S_4]^{2+/3+}$ ($E_{1/2}$ = **7**, 0.08 V; **8**, −0.25 V) and $[Fe_4S_4]^{1+/2+}$ ($E_{1/2}$ = **7**, −1.33 V; **8**, −1.66 V) couples. The ∼300 mV cathodic shift of these processes for **8** as compared to **7** reflects the increased donicity of CH_3^- as compared to Cl^- and is consistent with what we observed for **1**.[27]

The electrochemical data recorded for **7** and **8** suggested that preparative isolation of $[7]^+$ or $[8]^+$ might be possible. Treatment of **8** with 1 equiv of $[Fc][B(C_6F_5)_4]$ (Fc = ferrocene) in DFB produced an intense purple solution of the corresponding cation, $[8]^+$, which could be isolated from the reaction mixture in 84% yield. Although $[8]^+$ is stable in the solid state at −35 °C under an inert atmosphere, DFB or CD_2Cl_2 solutions of $[8]^+$ decompose over hours at room temperature (rt) to complex mixtures of products. Attempts to dissolve $[8]^+$ in coordinating solvents such as THF or Et_2O at rt resulted in immediate degradation to a multitude of species.

https://dx.doi.org/10.1021/jacs.0c06334
J. Am. Chem. Soc. 2020, 142, 14314−14323

Attempts to oxidize **7** under the same conditions produced only complex mixtures according to ^{1}H NMR spectra that were recorded immediately after mixing.

Given that $[\mathbf{8}]^+$ is the first isolated example of an alkylated $[Fe_4S_4]^{3+}$ cluster, we were interested to see how its EPR spectrum compares to those recorded for analogous biological intermediates.[7,8,16−19,23−26] The X-band EPR spectrum of $[\mathbf{8}]^+$ consists of a pseudoaxial signal that can be simulated with g = [2.101, 2.050, 2.042] (g_{iso} = 2.064; Figure 4); no other EPR

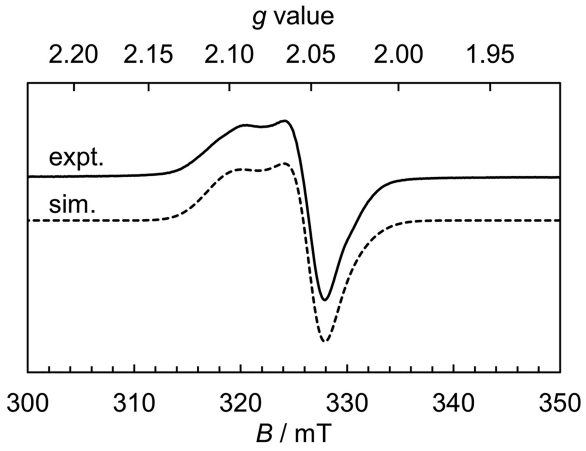

Figure 4. CW EPR spectrum of $[\mathbf{8}][B(C_6F_5)_4]$ recorded at 9.37 GHz and 0.05 mW power in an *o*-difluorobenzene glass at 30 K. Simulation parameters: g, [2.10, 2.05, 2.04]; g-strain, [0.035, 0.045, 0.015]; H-strain, [54 32 0] MHz.

signals were observed in spectra recorded as low as 5 K, which indicates that no higher-spin excited states are significantly populated at low temperature. Partially resolved hyperfine coupling (presumably to the ^{14}N nuclei of the NIm donors) was also observed. These data demonstrate that $[\mathbf{8}]^+$ adopts the $S = {}^1/_2$ ground state typical of synthetic thiolate-ligated $[Fe_4S_4]^{3+}$ clusters[31,48] and oxidized high potential iron−sulfur proteins (HiPIPs),[49−53] which display similar g_{iso} values in the range of 2.04−2.08. Likewise, all enzymatic $[Fe_4S_4]^{3+}$−alkyl intermediates thus far characterized exhibit a doublet ground state with $g_{iso} > 2$;[7,8,16−19,23−26] that $[\mathbf{8}]^+$, a well-defined $[Fe_4S_4]^{3+}$−alkyl cluster, also exhibits $g_{iso} > 2$ lends supports to the structural assignments made for these transient intermediates. Interestingly, the ferraoxetane intermediate for IspG (Scheme 1A) displays a similar isotropic g value (g_{iso} = 2.035) and similar rhombicity,[7,16−18] whereas the organometallic intermediates proposed for canonical and noncanonical radical SAM enzymes (Scheme 1B and C) feature lower g_{iso} values of ∼2.015 and less rhombicity.[8,23−25] These discrepancies may be in part due to the local protein environment and/or the differences in the coordination number of the alkylated Fe. More detailed EPR spectroscopic studies of $[\mathbf{8}]^+$ and of higher-coordinate derivatives are underway to further resolve these questions.

Although $[\mathbf{8}]^+$ is unstable in solution (vide supra), its degradation is sufficiently slow at −35 °C to permit growth of single crystals suitable for XRD studies (Figure 5). A comparative analysis of the structures of **8** and $[\mathbf{8}]^+$ is shown in Figure 6. As expected from trends between reported $[Fe_4S_4]^{2+}$ and $[Fe_4S_4]^{3+}$ clusters,[12,28−32] the cluster bond lengths generally contract upon oxidation of **8**: the average Fe−N distance decreases from 1.989(3) to 1.940(5) Å, the

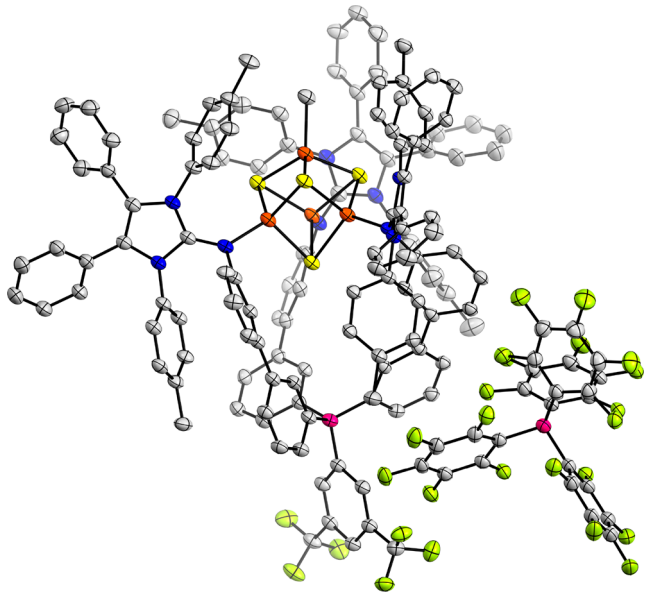

Figure 5. Thermal ellipsoid plot (30%) of $[\mathbf{8}][B(C_6F_5)_3]$. The coloring scheme is the same as that in Figure 1. Hydrogen atoms and solvent molecules are omitted for clarity.

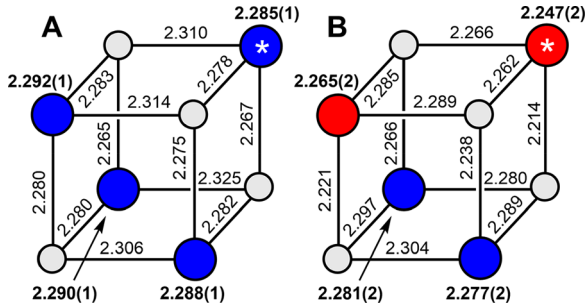

Figure 6. Schematics of the Fe_4S_4 cores showing Fe−S distances for (A) **8** and (B) $[\mathbf{8}][B(C_6F_5)_4]$ as determined by XRD. Large spheres = Fe, small gray spheres = S. The average Fe−S bond lengths (Å) for each site are shown in bold. The spheres marked with asterisks represent the alkylated Fe sites. Fe sites are colored according to their assigned solid-state valences: $Fe^{2.5+}$ = blue, Fe^{3+} = red. Standard uncertainties from individual Fe−S distances have been omitted for clarity; uncertainties for average distances here and elsewhere are given as the root sum of the squares of the individual estimated standard deviations.

Fe−CH_3 distance decreases from 2.026(3) to 2.000(4) Å, and the cluster core contracts slightly as evident from the Fe−S bonds, which shorten from an average 2.289(2) to 2.268(3) Å. In contrast to **8**, for which every Fe site has nearly identical average Fe−S distances, $[\mathbf{8}]^+$ displays distinct asymmetry. The CH_3-ligated Fe and, to a lesser extent, one of the NIm-bound Fe ions feature the shortest Fe−S bonds (averages of 2.247(2) and 2.265(2) Å, respectively); the two remaining NIm-bound Fe sites exhibit longer Fe−S bonds that are similar to those in **8** (2.281(2) and 2.277(2) Å). Given the empirical relationship between average Fe−S bond lengths and formal valence,[54] this divergence of local bond metrics for $[\mathbf{8}]^+$ is consistent with, formally, 2 × $Fe^{2.5+}$ and 2 × Fe^{3+} sites as described by the Heisenberg double-exchange model applied to the $[Fe_4S_4]^{3+}$ core,[55] with the alkylated Fe and an NIm-bound, spin-aligned Fe assigned to the two Fe^{3+} sites. The remaining NIm-bound

https://dx.doi.org/10.1021/jacs.0c06334
J. Am. Chem. Soc. 2020, 142, 14314−14323

centers that exhibit longer Fe−S bonds are then designated as the 2 × $Fe^{2.5+}$ pair engaging in a double-exchange interaction.

The hypothesis that the alkylated Fe site adopts an Fe^{3+} valence can be tested using ^{57}Fe Mössbauer spectroscopy. This electronic-structure model would yield a 1:1:2 pattern of isomer shifts (in order of increasing isomer shift) with the lowest isomer shift corresponding to the alkylated Fe site, an intermediate isomer shift corresponding to the other Fe^{3+} site, and the two highest isomer shifts corresponding to the $Fe^{2.5+}$ sites.[27] In contrast, an electronic-structure model in which the alkylated Fe site is one of the $Fe^{2.5+}$ sites would yield a 1:2:1 pattern of the alkylated Fe site, two Fe^{3+} sites, and one $Fe^{2.5+}$ site. We therefore acquired and analyzed the Mössbauer spectra of **7**, **8**, and $[\mathbf{8}]^+$. These data, and what we have determined to be their most reasonable simulations, are shown in Figure 7; other possible simulations and detailed reasoning behind our rationale are given in the Supporting Information. A summary of important experimental and calculated parameters is given in Table 1.

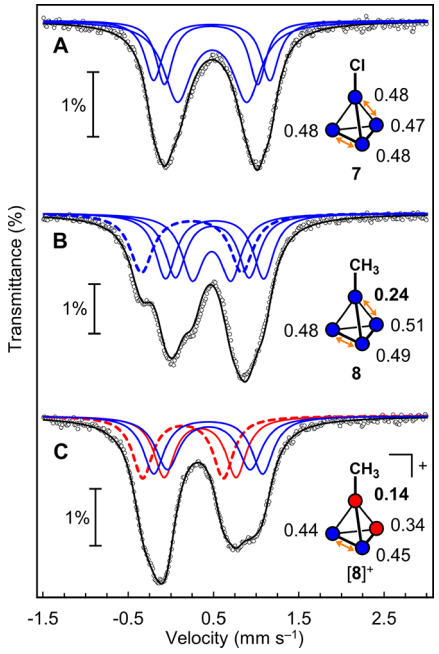

Figure 7. Zero-field ^{57}Fe Mössbauer spectra (80 K) of (A) **7**, (B) **8**, and (C) $[\mathbf{8}]^+$. Schematics: Each Fe center is represented by a sphere; those whose ligands are not shown are bound by $[L^B(NIm)_3]^-$; numbers correspond to isomer shifts (mm s^{-1}); double-exchange interactions are indicated by orange arrows. Spectra and simulations: black circles = experimental data; total simulation = black line; solid and dashed lines represent simulations of NIm/Cl^-- and CH_3-ligated sites, respectively. For both the simulations and the schematics, blue = $Fe^{2.5+}$ and red = Fe^{3+}.

The Mössbauer spectrum of **7**, which formally consists of 4 × $Fe^{2.5+}$ sites, is symmetrical about an average isomer shift of 0.48 mm s^{-1}; this value is comparable to those reported for $[Fe_4S_4(SR)_4]^{2-}$ clusters,[12] which further underscores the similar electronic properties of neutral imidazolinimine and anionic thiolate donors for Fe_4S_4 clusters.[40] The Mössbauer spectrum of **8** exhibits decreased symmetry as compared to that of **7**: two Fe sites show essentially unchanged isomer shifts of ∼0.48 mm s^{-1}; one is increased slightly to 0.51 mm s^{-1}, and another, that of the alkylated site, is sharply decreased to 0.24 mm s^{-1}. On the basis of our previous work, we attribute this to a combination of two effects: (1) more covalent bonding between Fe and CH_3 as compared to Fe and Cl, which (2) results in partial valence localization between the alkylated site and its double-exchange-coupled partner (see the Supporting Information for further discussion).[27,56] Upon oxidation to $[\mathbf{8}]^+$, two Fe sites continue to display isomer shifts consistent with $Fe^{2.5+}$ (∼0.45 mm s^{-1}) with the slight decrease as compared to **7** and **8** attributed to the overall contraction of the Fe−S core as expected upon oxidation.[11] The remaining two doublets show markedly lower isomer shifts of 0.34 mm s^{-1} and, most dramatically, 0.14 mm s^{-1}. The former value is similar to that reported for $[Fe_4S_4(SR)_4]^-$ clusters and is assigned to the Fe^{3+}−NIm site;[12,48,51,57,58] the latter doublet is therefore assigned to the alkylated Fe^{3+}. The isomer shift for the methyl-bound Fe in $[\mathbf{8}]^+$ is among the lowest observed for a tetrahedral site in an Fe−S cluster;[59,60] for comparison, the all-ferric cluster $Fe_4S_4(N(TMS)_2)_4$, which features a more oxidized, $[Fe_4S_4]^{4+}$ core, displays an isomer shift of 0.26 mm s^{-1}.[29]

To corroborate these assignments for the Mössbauer spectra of **8** and $[\mathbf{8}]^+$, we calculated theoretical spectra using broken-symmetry density functional theory (BS DFT) methods (Table 1). For both **8** and $[\mathbf{8}]^+$, the lowest-energy BS determinants correspond to the electronic-structure pictures proposed above. For **8**, we calculate δ = 0.48 and 0.49 mm s^{-1} for the double-exchange-coupled NIm-ligated pair, and δ = 0.52 and 0.22 mm s^{-1} for the remaining NIm-ligated Fe and the methylated Fe, respectively. The lowest-energy BS solution of $[\mathbf{8}]^+$ predicts that a pair of NIm-ligated sites remains as a valence-delocalized $Fe^{2.5+}$−$Fe^{2.5+}$ pair with δ = 0.41 mm s^{-1} and that the remaining NIm-ligated site and the methylated site are oxidized to Fe^{3+}, with δ = 0.38 and 0.19 mm s^{-1}, respectively. All of the calculated isomer shifts are in good agreement with experiment. Moreover, the site-specific valence assignments predicted by this solution are in agreement with those made on the basis of our XRD analysis (vide supra).

Taken together, the structural, spectroscopic, and computational data obtained for $[\mathbf{8}]^+$ indicate localization of Fe^{3+} at the alkylated Fe, which suggests that the strongly donating alkyl ligand raises the energy of the local 3d manifold and destabilizes relatively more reduced configurations at this

Table 1. Selected Simulation and Computed Zero-Field ^{57}Fe Mössbauer Parameters for the Spectra Shown in Figure 7[a]

	7 (X = Cl)			**8** (X = CH_3)			$[\mathbf{8}]^+$ (X = CH_3)		
site[b]	δ	$\lvert\Delta E_Q\rvert$	Γ	δ	$\lvert\Delta E_Q\rvert$	Γ	δ	$\lvert\Delta E_Q\rvert$	Γ
Fe−X (A)	0.48	1.36	0.25	0.24 (0.22)	1.18	0.32	0.14 (0.19)	0.95	0.29
Fe−N (A)	0.47	1.10	0.24	0.51 (0.52)	1.15	0.29	0.34 (0.38)	0.84	0.29
Fe−N (B)	0.48	0.82	0.40	0.48 (0.48)	0.45	0.30	0.45 (0.41)	0.97	0.34
Fe−N (B)	0.48	0.82	0.40	0.49 (0.47)	0.87	0.30	0.44 (0.41)	1.28	0.30

[a]All values are in units of mm s^{-1}. [b](b) Pairs of spin-aligned sites are indicated by (A) or (B). Numbers in parentheses are calculated values.

https://dx.doi.org/10.1021/jacs.0c06334
J. Am. Chem. Soc. 2020, 142, 14314−14323

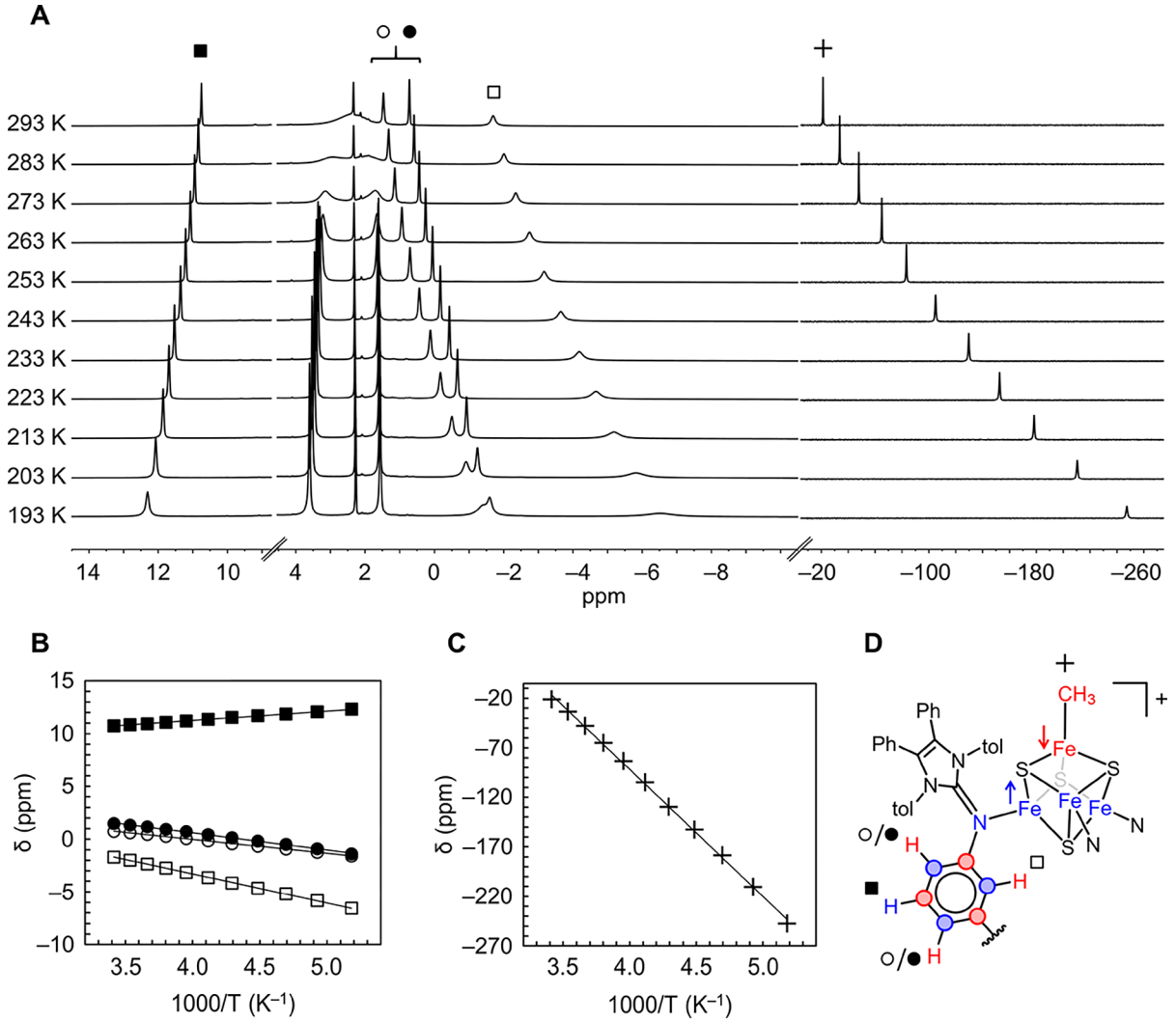

Figure 8. ^{1}H NMR spectra (A) recorded for $[\mathbf{8}]^+$ between 193 and 293 K; plots of chemical shift versus inverse temperature for (B) selected aryl and (C) Fe−CH_3 protons; (D) labeling scheme for the data presented herein: ↑ and ↓ correspond to spins aligned parallel and antiparallel with the NMR magnetic field, respectively; and red and blue atoms harbor minority and majority spin, respectively.

site. At cryogenic temperatures, solid samples of homoleptic $[Fe_4S_4]^{3+}$ clusters also exhibit valence localization as is evident in their X-ray crystallographic[28−32] and Mössbauer spectroscopic[29,48] properties. However, the ^{1}H NMR spectra of these clusters invariably show a single set of resonances for each ligand,[29,31,32] which indicates that on the NMR time scale the rate of intramolecular electron transfer, which exchanges the $Fe^{2.5+}$ and Fe^{3+} pairs, is fast, to produce an averaged valence of 2.75+ at each site. To learn if this behavior is also observed for $[\mathbf{8}]^+$ or if this cluster would exhibit valence localization in solution, which, to our knowledge, has not been previously observed for a synthetic $[Fe_4S_4]^{3+}$ cluster, we undertook analysis of its solution NMR properties.

Our approach to answering this question was to use the sign of the paramagnetic shifts of the ^{1}H resonances for $[\mathbf{8}]^+$ to infer whether each Fe center bears majority spin (parallel with the external magnetic field) or minority spin (antiparallel with the external magnetic field). Such information reports on the Fe valence because, in the ground states of $[Fe_4S_4]^{3+}$ clusters, it has been established that the $Fe^{2.5+}$ and the Fe^{3+} sites harbor majority and minority spin, respectively.[48,57] This is reflected in the ^{1}H NMR spectra of protein-bound $[Fe_4S_4]^{3+}$ clusters, which feature two sets of β-cysteinyl resonances that have opposing temperature dependence: those bound to the $Fe^{2.5+}$ sites are shifted downfield, and those bound to the Fe^{3+} sites are shifted upfield.[61−63] As discussed above, solution samples of synthetic $[Fe_4S_4]^{3+}$ clusters do not display this valence localization: their Fe sites rapidly convert between $Fe^{2.5+}$ (majority spin) and Fe^{3+} (minority spin), to result in net majority spin on each Fe site. Given this precedent, we expected that if $[\mathbf{8}]^+$ behaves like all other synthetic $[Fe_4S_4]^{3+}$ clusters, then each Fe site would appear by ^{1}H NMR spectroscopy to harbor net majority spin. On the other hand, if the methyl group localizes Fe^{3+} at the alkylated Fe site, then this Fe site would bear minority spin and the other three formally $Fe^{2.67+}$ sites would bear majority spin.

To distinguish these possibilities, we recorded ^{1}H NMR spectra of $[\mathbf{8}]^+$ in CD_2Cl_2 over a 100 K range. The room-temperature spectrum features paramagnetically shifted resonances between −20 and +12 ppm (Figure 8A). Four aryl ^{1}H resonances, each integrating for three protons, are shifted substantially from their diamagnetic chemical shifts (∼7 ppm) and were assigned to the 2-, 4-, 5-, and 6-protons of the NIm-bound aryl ring on the basis of ^{1}H−^{1}H COSY experiments

https://dx.doi.org/10.1021/jacs.0c06334
J. Am. Chem. Soc. 2020, 142, 14314−14323

(Figure S29). The 2-, 4-, and 6-protons are shifted negatively, and the 5-proton is shifted positively; each exhibits Curie behavior in variable-temperature studies (Figure 8B). This alternating spin pattern in which the protons in an *ortho*- or *para*-position relative to the NIm N donor are shifted negatively and those in a *meta*-position are shifted positively is the same as that observed for the aryl protons in $[Fe_4S_4(SAr)_4]^{n-}$ (n = 1−3) clusters.[31,43−46] In these clusters as well as in $[\mathbf{8}]^+$, this pattern indicates majority spin density on the Fe center to which the donor group is bound; spin delocalization onto the donor atom via both σ and π bonding results in majority spin on the donor atom, which then polarizes the spins on adjacent C/H atoms in an alternating fashion (Figure 8D).[64] This analysis is also supported by calculated spin densities in mononuclear $[NImFeCl_3]^{0/-}$ model complexes (Figure S42).

For the methyl protons in $[\mathbf{8}]^+$, we would expect their ^{1}H NMR resonances to be shifted downfield if the alkylated Fe harbors majority spin. We reach this conclusion on the basis of the ^{2}H NMR chemical shift for the Fe−CD_3 deuterons in the tetrahedral, high-spin mononuclear complex $TpFeCD_3$ (Tp = (tris(3-*tert*-butylpyrazolyl)phenylborate), which occurs at 1453 ppm (293 K),[65,66] and also on the basis of calculated spin densities for mononuclear $[FeCl_3CH_3]^{0/-}$ model complexes that show spin delocalization onto the H atoms (Figure S42). Strikingly, however, the Fe−CH_3 proton resonances for $[\mathbf{8}]^+$ (identified by comparison with its Fe−CD_3 isotopologue; see Figure S28) appear at −20 ppm at 293 K and shift to −248 at 193 K with approximate Curie behavior (Figure 8C). The upfield chemical shift of the Fe−CH_3 protons in $[\mathbf{8}]^+$ indicates that the alkylated Fe site harbors localized minority spin density, which, to the best of our knowledge, has not been observed for any other synthetic $[Fe_4S_4]^{3+}$ cluster for which NMR data are available.[29,31] Overall, we conclude that the electronic structure of $[\mathbf{8}]^+$ at ambient temperature is best described as having a valence-localized Fe^{3+}−CH_3 site, with the other three sites rapidly interconverting between $Fe^{2.5+}$ and Fe^{3+} to give an effective valence of +2.67 for each (Figure 9).

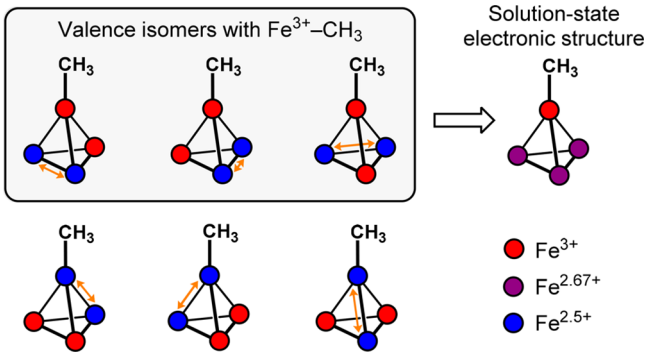

Figure 9. Possible valence isomers (left) and effective valences in solution for $[\mathbf{8}]^+$ (right).

Calculations further validate this unusual electronic assignment; detailed methodologies and discussion are given in the Supporting Information. In summary, models assuming full valence delocalization (i.e., all Fe sites are averaged as $Fe^{2.75+}$) consistently predict that resonances for the Fe−CH_3 protons will shift downfield with decreasing temperature, which contradicts experiment (Figure S43). In contrast, models with a valence-localized Fe^{3+}−CH_3 site and 3× valence-delocalized $Fe^{2.67+}$ sites qualitatively reproduce the temperature dependence of ^{1}H shifts observed for $[\mathbf{8}]^+$ (Figures S44 and S45).

On the basis of these results, we propose that future studies of enzymatic $[Fe_4S_4]^{3+}$−alkyl intermediates take into consideration the strong likelihood of valence localization at the alkylated Fe site, both at cryogenic temperatures (at which such intermediates are typically characterized) and at physiologically relevant temperatures. The observation that the alkyl ligand induces valence localization even in the absence of a protein environment highlights the ability of strong-field ligands to impart unusual electronic structures to Fe−S clusters.

CONCLUSIONS

We have described the isolation and characterization of the first $[Fe_4S_4]^{3+}$−alkyl cluster, a synthetic model of organometallic intermediates proposed in terpene biosynthesis, radical SAM catalysis, and dipthamide biosynthesis. Although this species reacts rapidly with even weakly coordinating donor solvents and slowly degrades in solution at room temperature, it is stable in the solid state and sufficiently stable in solution to allow for its complete characterization. The alkylated Fe site has an unusually low Mössbauer isomer shift, which may prove to be a spectroscopic signature for $[Fe_4S_4]^{3+}$−alkyl intermediates. The low isomer shift and contracted Fe−S bonds of the alkylated Fe site indicate that it is best described as Fe^{3+} in the solid state. Surprisingly, this valence localization persists in solution at room temperature. Taken together, these results suggest that the electronic structures of enzymatic $[Fe_4S_4]^{3+}$−alkyl intermediates may also exhibit valence localization at the alkylated Fe site. Both $[\mathbf{8}]^+$ and the reported enzymatic $[Fe_4S_4]^{3+}$−alkyl intermediates exhibit EPR signals with $g_{iso} > 2$; variability in the magnitude of the shift from g_e may reflect differences in the coordination number or geometry at the unique Fe site. Further efforts will be directed at making analogues of $[\mathbf{8}]^+$ that will allow us to delineate how coordination number/geometry of this Fe site impacts the electronic structure and reactivity of the cluster. Finally, we emphasize that this study was enabled by the stabilization of the $[Fe_4S_4]^{3+}$−alkyl core by an expanded scorpionate ligand. We anticipate that further application of this strategy to the chemistry of metalloclusters will enable the isolation of other unusual and reactive species.

ASSOCIATED CONTENT

Supporting Information

The Supporting Information is available free of charge at https://pubs.acs.org/doi/10.1021/jacs.0c06334.

Experimental procedures and characterization data for all of the new products (PDF)
Crystallographic data for **2** (CIF)
Crystallographic data for **7** (CIF)
Crystallographic data for **8** (CIF)
Crystallographic data for $[\mathbf{8}][B(C_6F_5)_4]$ (CIF)

AUTHOR INFORMATION

Corresponding Author

Daniel L. M. Suess − *Department of Chemistry, Massachusetts Institute of Technology, Cambridge, Massachusetts 02139, United States;* orcid.org/0000-0002-0916-1973; Email: suess@mit.edu

https://dx.doi.org/10.1021/jacs.0c06334
J. Am. Chem. Soc. 2020, 142, 14314−14323

Authors

Alex McSkimming − *Department of Chemistry, Massachusetts Institute of Technology, Cambridge, Massachusetts 02139, United States*

Arun Sridharan − *Department of Chemistry, Massachusetts Institute of Technology, Cambridge, Massachusetts 02139, United States;* orcid.org/0000-0001-9249-8894

Niklas B. Thompson − *Department of Chemistry, Massachusetts Institute of Technology, Cambridge, Massachusetts 02139, United States;* orcid.org/0000-0003-2745-4945

Peter Müller − *Department of Chemistry, Massachusetts Institute of Technology, Cambridge, Massachusetts 02139, United States;* orcid.org/0000-0001-6530-3852

Complete contact information is available at: https://pubs.acs.org/10.1021/jacs.0c06334

Notes

The authors declare no competing financial interest.

■ ACKNOWLEDGMENTS

Research reported here was supported in part by the National Institute of General Medical Sciences of the National Institutes of Health under award number R01GM136882 and under a fellowship for N.B.T. (award number F32GM137478).

■ REFERENCES

(1) Flint, D. H.; Allen, R. M. Iron-Sulfur Proteins with Nonredox Functions. *Chem. Rev.* **1996**, *96* (7), 2315−2334.

(2) Beinert, H.; Holm, R. H.; Munck, E. Iron-Sulfur Clusters: Nature's Modular, Multipurpose Structures. *Science* **1997**, *277* (5326), 653−659.

(3) Rees, D. C.; Howard, J. B. The Interface between the Biological and Inorganic Worlds: Iron-Sulfur Metalloclusters. *Science* **2003**, *300* (5621), 929−931.

(4) Johnson, D. C.; Dean, D. R.; Smith, A. D.; Johnson, M. K. Structure, Function, and Formation of Biological Iron-Sulfur Clusters. *Annu. Rev. Biochem.* **2005**, *74*, 247−281.

(5) Can, M.; Armstrong, F. A.; Ragsdale, S. W. Structure, Function, and Mechanism of the Nickel Metalloenzymes, CO Dehydrogenase, and Acetyl-CoA Synthase. *Chem. Rev.* **2014**, *114* (8), 4149−4174.

(6) Hoffman, B. M.; Lukoyanov, D.; Yang, Z. Y.; Dean, D. R.; Seefeldt, L. C. Mechanism of Nitrogen Fixation by Nitrogenase: The Next Stage. *Chem. Rev.* **2014**, *114* (8), 4041−4062.

(7) Wang, W. X.; Oldfield, E. Bioorganometallic Chemistry with IspG and IspG: Structure, Function, and Inhibition of the $[Fe_4S_4]$ Proteins Involved in Isoprenoid Biosynthesis. *Angew. Chem., Int. Ed.* **2014**, *53* (17), 4294−4310.

(8) Broderick, W. E.; Hoffman, B. M.; Broderick, J. B. Mechanism of Radical Initiation in the Radical S-Adenosyl-L-Methionine Superfamily. *Acc. Chem. Res.* **2018**, *51* (11), 2611−2619.

(9) Cammack, R. Iron-Sulfur Clusters in Enzymes - Themes and Variations. *Adv. Inorg. Chem.* **1992**, *38*, 281−322.

(10) Hagen, W. R. EPR Spectroscopy of Iron-Sulfur Proteins. *Adv. Inorg. Chem.* **1992**, *38*, 165−222.

(11) Pandelia, M. E.; Lanz, N. D.; Booker, S. J.; Krebs, C. Mössbauer Spectroscopy of Fe/S Proteins. *Biochim. Biophys. Acta, Mol. Cell Res.* **2015**, *1853* (6), 1395−1405.

(12) Venkateswara Rao, P.; Holm, R. H. Synthetic Analogues of the Active Sites of Iron-Sulfur Proteins. *Chem. Rev.* **2004**, *104* (2), 527−559.

(13) Lee, S. C.; Holm, R. H. The Clusters of Nitrogenase: Synthetic Methodology in the Construction of Weak-Field Clusters. *Chem. Rev.* **2004**, *104* (2), 1135−1157.

(14) Lee, S. C.; Lo, W.; Holm, R. H. Developments in the Biomimetic Chemistry of Cubane-Type and Higher Nuclearity Iron-Sulfur Clusters. *Chem. Rev.* **2014**, *114* (7), 3579−3600.

(15) Holm, R. H.; Lo, W. Structural Conversions of Synthetic and Protein-Bound Iron-Sulfur Clusters. *Chem. Rev.* **2016**, *116* (22), 13685−13713.

(16) Xu, W. Y.; Lees, N. S.; Adedeji, D.; Wiesner, J.; Jomaa, H.; Hoffman, B. M.; Duin, E. C. Paramagnetic Intermediates of (E)-4-Hydroxy-3-methylbut-2-enyl Diphosphate Synthase (GcpE/IspG) under Steady-State and Pre-Steady-State Conditions. *J. Am. Chem. Soc.* **2010**, *132* (41), 14509−14520.

(17) Xu, W. Y.; Lees, N. S.; Hall, D.; Welideniya, D.; Hoffman, B. M.; Duin, E. C. A Closer Look at the Spectroscopic Properties of Possible Reaction Intermediates in Wild-Type and Mutant (E)-4-Hydroxy-3-methylbut-2-enyl Diphosphate Reductase. *Biochemistry* **2012**, *51* (24), 4835−4849.

(18) Wang, W. X.; Li, J. K.; Wang, K.; Huang, C. C.; Zhang, Y.; Oldfield, E. Organometallic Mechanism of Action and Inhibition of the 4Fe-4S Isoprenoid Biosynthesis Protein GcpE (IspG). *Proc. Natl. Acad. Sci. U. S. A.* **2010**, *107* (25), 11189−11193.

(19) Wang, W. X.; Wang, K.; Li, J. K.; Nellutla, S.; Smirnova, T. I.; Oldfield, E. An ENDOR and HYSCORE Investigation of a Reaction Intermediate in IspG (GcpE) Catalysis. *J. Am. Chem. Soc.* **2011**, *133* (22), 8400−8403.

(20) Sofia, H. J.; Chen, G.; Hetzler, B. G.; Reyes-Spindola, J. F.; Miller, N. E. Radical SAM, a Novel Protein Superfamily Linking Unresolved Steps in Familiar Biosynthetic Pathways with Radical Mechanisms: Functional Characterization Using New Analysis and Information Visualization Methods. *Nucleic Acids Res.* **2001**, *29* (5), 1097−1106.

(21) Broderick, J. B.; Duffus, B. R.; Duschene, K. S.; Shepard, E. M. Radical S-Adenosylmethionine Enzymes. *Chem. Rev.* **2014**, *114* (8), 4229−4317.

(22) Holliday, G. L.; Akiva, E.; Meng, E. C.; Brown, S. D.; Calhoun, S.; Pieper, U.; Sali, A.; Booker, S. J.; Babbitt, P. C. Atlas of the Radical SAM Superfamily: Divergent Evolution of Function Using a "Plug and Play" Domain. *Methods Enzymol.* **2018**, *606*, 1−71.

(23) Horitani, M.; Shisler, K.; Broderick, W. E.; Hutcheson, R. U.; Duschene, K. S.; Marts, A. R.; Hoffman, B. M.; Broderick, J. B. Radical SAM Catalysis via an Organometallic Intermediate with an Fe-[5′-C]-Deoxyadenosyl Bond. *Science* **2016**, *352* (6287), 822−825.

(24) Byer, A. S.; Yang, H.; McDaniel, E. C.; Kathiresan, V.; Impano, S.; Pagnier, A.; Watts, H.; Denler, C.; Vagstad, A. L.; Piel, J.; Duschene, K. S.; Shepard, E. M.; Shields, T. P.; Scott, L. G.; Lilla, E. A.; Yokoyama, K.; Broderick, W. E.; Hoffman, B. M.; Broderick, J. B. Paradigm Shift for Radical S-Adenosyl-L-Methionine Reactions: The Organometallic Intermediate Omega Is Central to Catalysis. *J. Am. Chem. Soc.* **2018**, *140* (28), 8634−8638.

(25) Dong, M.; Kathiresan, V.; Fenwick, M. K.; Torelli, A. T.; Zhang, Y.; Caranto, J. D.; Dzikovski, B.; Sharma, A.; Lancaster, K. M.; Freed, J. H.; Ealick, S. E.; Hoffman, B. M.; Lin, H. N. Organometallic and Radical Intermediates Reveal Mechanism of Diphthamide Biosynthesis. *Science* **2018**, *359* (6381), 1247−1250.

(26) Yang, H.; Impano, S.; Shepard, E. M.; James, C. D.; Broderick, W. E.; Broderick, J. B.; Hoffman, B. M. Photoinduced Electron Transfer in a Radical SAM Enzyme Generates an S-Adenosylmethionine Derived Methyl Radical. *J. Am. Chem. Soc.* **2019**, *141* (40), 16117−16124.

(27) Ye, M.; Thompson, N. B.; Brown, A. C.; Suess, D. L. M. A Synthetic Model of Enzymatic $[Fe_4S_4]$-Alkyl Intermediates. *J. Am. Chem. Soc.* **2019**, *141* (34), 13330−13335.

(28) Osullivan, T.; Millar, M. M. Synthesis and Study of an Analog for the $[Fe_4S_4]^{3+}$ Center of Oxidized High-Potential Iron-Sulfur Proteins. *J. Am. Chem. Soc.* **1985**, *107* (13), 4096−4097.

(29) Sharp, C. R.; Duncan, J. S.; Lee, S. C. $[Fe_4S_4]^{Q}$ Cubane Clusters (Q = 4+, 3+, 2+) with Terminal Amide Ligands. *Inorg. Chem.* **2010**, *49* (14), 6697−6705.

(30) Ohki, Y.; Tanifuji, K.; Yamada, N.; Imada, M.; Tajima, T.; Tatsumi, K. Synthetic Analogues of $[Fe_4S_4(Cys)_3(His)]$ in Hydro-

genases and $[Fe_4S_4(Cys)_4]$ in HiPIP Derived from All-Ferric $[Fe_4S_4\{N(SiMe_3)_2\}_4]$. *Proc. Natl. Acad. Sci. U. S. A.* **2011**, *108* (31), 12635−12640.
(31) Tanifuji, K.; Yamada, N.; Tajima, T.; Sasamori, T.; Tokitoh, N.; Matsuo, T.; Tamao, K.; Ohki, Y.; Tatsumi, K. A Convenient Route to Synthetic Analogues of the Oxidized Form of High-Potential Iron-Sulfur Proteins. *Inorg. Chem.* **2014**, *53* (8), 4000−4009.
(32) Tanifuji, K.; Tajima, S.; Ohki, Y.; Tatsumi, K. Interconversion between $[Fe_4S_4]$ and $[Fe_2S_2]$ Clusters Bearing Amide Ligands. *Inorg. Chem.* **2016**, *55* (9), 4512−4518.
(33) Smith, J. Strongly Donating Scorpionate Ligands. *Comments Inorg. Chem.* **2008**, *29* (5−6), 189−233.
(34) Trofimenko, S. Recent Advances in Poly(Pyrazolyl)Borate (Scorpionate) Chemistry. *Chem. Rev.* **1993**, *93* (3), 943−980.
(35) Saouma, C. T.; Peters, J. C. M≡E and M = E Complexes of Iron and Cobalt That Emphasize Three-Fold Symmetry (E O, N, NR). *Coord. Chem. Rev.* **2011**, *255* (7−8), 920−937.
(36) Ge, P. H.; Haggerty, B. S.; Rheingold, A. L.; Riordan, C. G. Poly(methylthiomethyl)borates - a New Class of Sulfur-Rich Ligands for Metal-Ions. *J. Am. Chem. Soc.* **1994**, *116* (18), 8406−8407.
(37) Spicer, M. D.; Reglinski, J. Soft Scorpionate Ligands Based on Imidazole-2-thione Donors. *Eur. J. Inorg. Chem.* **2009**, *2009* (12), 1553−1574.
(38) Stack, T. D. P.; Holm, R. H. Subsite-Specific Functionalization of the $[4Fe\text{-}4S]^{2+}$ Analog of Iron Sulfur Protein Clusters. *J. Am. Chem. Soc.* **1987**, *109* (8), 2546−2547.
(39) Stack, T. D. P.; Holm, R. H. Subsite-Differentiated Analogs of Biological $[4Fe\text{-}4S]^{2+}$ Clusters - Synthesis, Solution and Solid-State Structures, and Subsite-Specific Reactions. *J. Am. Chem. Soc.* **1988**, *110* (8), 2484−2494.
(40) McSkimming, A.; Suess, D. L. M. Selective Synthesis of Site-Differentiated Fe_4S_4 and Fe_6S_6 Clusters. *Inorg. Chem.* **2018**, *57* (23), 14904−14912.
(41) Walsdorff, C.; Saak, W.; Pohl, S. A New Preorganized Tridentate Ligand Bearing Three Indolethiolate Groups. Preparation of 3:1 Subsite-Differentiated Fe_4S_4 Clusters. *J. Chem. Soc., Dalton Trans.* **1997**, No. 11, 1857−1861.
(42) Terada, T.; Wakimoto, T.; Nakamura, T.; Hirabayashi, K.; Tanaka, K.; Li, J.; Matsumoto, T.; Tatsumi, K. Tridentate Thiolate Ligands: Application to the Synthesis of the Site-Differentiated [4Fe-4S] Cluster Having a Hydrosulfide Ligand at the Unique Iron Center. *Chem. - Asian J.* **2012**, *7* (5), 920−929.
(43) Holm, R. H.; Phillips, W. D.; Averill, B. A.; Mayerle, J. J.; Herskovitz, T. Synthetic Analogs of Active-Sites of Iron-Sulfur Proteins. 5. Proton-Resonance Properties of Tetranuclear Clusters $[Fe_4S_4(SR)_4]^{2-}$ - Evidence for Dominant Contact Interactions. *J. Am. Chem. Soc.* **1974**, *96* (7), 2109−2117.
(44) Reynolds, J. G.; Laskowski, E. J.; Holm, R. H. Proton Magnetic-Resonance Properties of Tetranuclear Clusters $[Fe_4S_4(SR)_4]^{3-}$, Analogs of 4-Fe Sites of Reduced Ferredoxins. *J. Am. Chem. Soc.* **1978**, *100* (17), 5315−5322.
(45) Weigel, J. A.; Holm, R. H. Intrinsic Binding-Properties of a Differentiated Iron Subsite in Analogs of Native $[Fe_4S_4]^{2+}$ Clusters. *J. Am. Chem. Soc.* **1991**, *113* (11), 4184−4191.
(46) Zhou, C. Y.; Holm, R. H. Comparative Isotropic Shifts, Redox Potentials, and Ligand Binding Propensities of [1:3] Site-Differentiated Cubane-type $[Fe_4Q_4]^{2+}$ Clusters (Q = S, Se). *Inorg. Chem.* **1997**, *36* (18), 4066−4077.
(47) Tsui, E. Y.; Day, M. W.; Agapie, T. Trinucleating Copper: Synthesis and Magnetostructural Characterization of Complexes Supported by a Hexapyridyl 1,3,5-Triarylbenzene Ligand. *Angew. Chem., Int. Ed.* **2011**, *50* (7), 1668−1672.
(48) Papaefthymiou, V.; Millar, M. M.; Münck, E. Mössbauer and Electron-Paramagnetic-Resonance Studies of a Synthetic Analog for the Fe_4S_4 Core of Oxidized and Reduced High-Potential Iron Proteins. *Inorg. Chem.* **1986**, *25* (17), 3010−3014.
(49) Antanaitis, B. C.; Moss, T. H. Magnetic Studies of the Four-Iron High-Potential, Non-Heme Protein from *Chromatium Vinosum*. *Biochim. Biophys. Acta, Protein Struct.* **1975**, *405* (2), 262−279.
(50) Beinert, H.; Thomson, A. J. Three-Iron Clusters in Iron-Sulfur Proteins. *Arch. Biochem. Biophys.* **1983**, *222* (2), 333−361.
(51) Bertini, I.; Campos, A. P.; Luchinat, C.; Teixeira, M. A Mössbauer Investigation of Oxidized Fe_4S_4 HiPIP-II from *Ectothiorhodospira-Halophila*. *J. Inorg. Biochem.* **1993**, *52* (3), 227−234.
(52) Cavazza, C.; Guigliarelli, B.; Bertrand, P.; Bruschi, M. Biochemical and EPR Characterization of a High-Potential Iron-Sulfur Protein in *Thiobacillus-Ferrooxidans*. *FEMS Microbiol. Lett.* **1995**, *130* (2−3), 193−199.
(53) Heering, H. A.; Bulsink, Y. B. M.; Hagen, W. R.; Meyer, T. E. Reversible Super-Reduction of the Cubane $[4Fe\text{-}4S]^{3+,2+,1+}$ in the High-Potential Iron-Sulfur Protein under Nondenaturing Conditions - EPR Spectroscopic and Electrochemical Studies. *Eur. J. Biochem.* **1995**, *232* (3), 811−817.
(54) Hoggins, J. T.; Steinfink, H. Empirical Bonding Relationships in Metal-Iron-Sulfide Compounds. *Inorg. Chem.* **1976**, *15* (7), 1682−1685.
(55) Noodleman, L.; Peng, C. Y.; Case, D. A.; Mouesca, J. M. Orbital Interactions, Electron Delocalization and Spin Coupling in Iron-Sulfur Clusters. *Coord. Chem. Rev.* **1995**, *144*, 199−244.
(56) Gütlich, P.; Bill, E.; Trautwein, A. X. Quantum Chemistry and Mössbauer Spectroscopy. *Mössbauer Spectroscopy and Transition Metal Chemistry*; Springer: Berlin, 2011; pp 137−199.
(57) Middleton, P.; Dickson, D. P. E.; Johnson, C. E.; Rush, J. D. Interpretation of the Mössbauer-Spectra of the High-Potential Iron Protein from *Chromatium*. *Eur. J. Biochem.* **1980**, *104* (1), 289−296.
(58) Moula, G.; Matsumoto, T.; Miehlich, M. E.; Meyer, K.; Tatsumi, K. Synthesis of an All-Ferric Cuboidal Iron-Sulfur Cluster $[(Fe_4S_4)(SAr)_4]$. *Angew. Chem., Int. Ed.* **2018**, *57* (36), 11594−11597.
(59) Sedney, D.; Reiff, W. M. Mössbauer-Spectroscopy Investigation of Iron Chromophore Equivalence in 3 Tetra-Iron Clusters. *Inorg. Chim. Acta* **1979**, *34* (2), 231−236.
(60) Chu, C. T. W.; Lo, F. Y. K.; Dahl, L. F. Synthesis and Stereochemical Analysis of the $[Fe_4(NO)_4(\mu_3\text{-}S)_4]^N$ Series (N = 0, −1) Which Possesses a Cubanelike Fe_4S_4 Core - Direct Evidence for the Antibonding Tetrametal Character of the Unpaired Electron Upon a One-Electron Reduction of a Completely Bonding Tetrahedral Metal Cluster. *J. Am. Chem. Soc.* **1982**, *104* (12), 3409−3422.
(61) Bertini, I.; Briganti, F.; Luchinat, C.; Scozzafava, A.; Sola, M. ^{1}H-NMR Spectroscopy and the Electronic-Structure of the High-Potential Iron Sulfur Protein from *Chromatium-Vinosum*. *J. Am. Chem. Soc.* **1991**, *113* (4), 1237−1245.
(62) Banci, L.; Bertini, I.; Briganti, F.; Luchinat, C.; Scozzafava, A.; Oliver, M. V. ^{1}H-NMR Spectra of Oxidized High-Potential Iron Sulfur Protein (HiPIP) from *Rhodocyclus-Gelatinosus* - a Model for Oxidized HiPIPs. *Inorg. Chem.* **1991**, *30* (24), 4517−4524.
(63) Banci, L.; Bertini, I.; Ciurli, S.; Ferretti, S.; Luchinat, C.; Piccioli, M. The Electronic-Structure of $[Fe_4S_4]^{3+}$ Clusters in Proteins - an Investigation of the Oxidized High-Potential Iron-Sulfur Protein-II from *Ectothiorhodospira-Vacuolata*. *Biochemistry* **1993**, *32* (36), 9387−9397.
(64) Bertini, I.; Luchinat, C.; Aime, S. NMR of Paramagnetic Substances. *Coord. Chem. Rev.* **1996**, *15*, 1−300.
(65) As $\delta \propto \gamma$, where γ is the gyromagnetic ratio of the nucleus being excited, and $\gamma(^1H)$, $\gamma(^2H) > 0$, the ^{1}H and ^{2}H shifts for $TpFeCD_3$ and $TpFeCH_3$ will be in the same direction.
(66) Kisko, J. L.; Hascall, T.; Parkin, G. The Synthesis, Structure and Reactivity of Phenyl Tris(3-*tert*-butylpyrazolyl)borato Iron Methyl, $[PhTp^{But}]FeMe$: Isolation of a Four-Coordinate Monovalent Iron Carbonyl Complex, $[PhTp^{But}]FeCO$. *J. Am. Chem. Soc.* **1998**, *120* (40), 10561−10562.

https://dx.doi.org/10.1021/jacs.0c06334
J. Am. Chem. Soc. 2020, 142, 14314−14323